Electronic Supplementary Material (ESI) for Sustainable Energy & Fuels.
This journal is © The Royal Society of Chemistry 2018

Methods

Precursor solution preparation and glovebox details

Perovskite precursor solutions were prepared in a nitrogen glovebox by dissolving appropriate ratios of Formamidinium Iodide (Dyesol), Cesium Iodide (Sigma Aldrich), Tin (II) Iodide (Sigma Aldrich, 99.999% beads), Lead (II) Iodide (TCI), in a mixed solvent comprising N,N-dimethylformamide (DMF, Sigma Aldrich) and Dimethylsulfoxide (DMSO, Sigma Aldrich) mixed in ratios by volume as described for particular perovskite solutions below. To all tin-containing perovskite solutions, Tin (II) Fluoride (Sigma Aldrich, 10 mol % of the amount of tin in the solution) was added to prevent formation of oxidized tin (IV) species. Perovskite solutions were filtered through a PTFE filter with 0.2um pore size prior to use. No heating was used to dissolve any solutions.

Polyethylenedioxythiophene:polystyrenesulfonate (PEDOT:PSS, Clevios P VP AI4083) was diluted 1:2 with methanol and filtered through a PVDF filter with pore size 0.2 um.

Polytriarylamine (PTAA, Solaris) was dissolved at a concentration of 5 mg/mL in chlorobenzene and filtered with a PTFE filter (0.2 um pore size)

Tin-containing perovskite films were fabricated in a nitrogen glovebox, while pure-lead perovskites were fabricated in a dry air glovebox. Both gloveboxes had moisture levels typically below 0.5 ppm, and the nitrogen glovebox had oxygen levels typically below 0.1 ppm. Gloveboxes were constantly purged during perovskite spin to prevent build-up of solvent vapors that might affect film crystallization.

Low Gap Single Junction Solar Cell Fabrication

ITO-coated glass substrates (10 ohm/sq., Xinyan Technologies) were cleaned by sonication in Extran detergent, acetone, and isopropanol successively, followed by UV-ozone treatment for approximately 15 minutes. PEDOT:PSS was spin coated at 5000 RPM for 25 seconds followed by heating at 150 C for 10 minutes, after which substrates were immediately transferred into a nitrogen glovebox.

For operational stability studies, perovskite of the desired composition was spun using a 1.5M solution in 85% DMF and 15% DMSO. The solution was deposited on PEDOT-coated substrates and spun at 5000 RPM (acceleration 5000 RPM/s). During the spin, 200 uL of diethyl ether antisolvent was dripped onto the spinning substrate. For perovskites with 60% tin, spin duration was 59 s and antisolvent was dripped at 12 s after starting the spin. For those with 40% tin, spin duration was 40s and antisolvent was dripped at 18 s. After the spin, the films were annealed at 100 C for 7 minutes.

The thick large grained low-gap perovskite was fabricated using a 2.0 M solution in 75% DMF, 25% DMSO. At least one hour prior to perovskite deposition, 5% by volume of formic acid (Sigma Aldrich, 95%) was added to the precursor solution. 15 uL of solution was deposited onto a PEDOT:PSS-coated substrate and spun at 3500 RPM for 25 seconds (acceleration 5000 RPM/s). Immediately after, the substrate (at this stage, still a clear light yellow wet layer) is immersed in a small petridish of anisole (Sigma Aldrich, anhydrous 99.7%), upon which the clear light yellow wet layer converts to brown within 1 – 2 seconds. After this the substrate is

blown dry with a nitrogen gun, kept at room temperature for 15 s, and then annealed at 100 C for 7 minutes.

MACl vapor treatment: The as-deposited films after the 100 C anneal were held for one minute 2 cm above an aluminium weigh boat containing methylammonium chloride powder kept on a hotplate at 150 C. Immediately after this MACl vapor exposure, each film was post-annealed at 150 C for a further one minute.

Following perovskite deposition, 40 nm of C_{60} (MER Corporation, 99.9% sublimed grade) and 7.5 nm of Bathocuproine (Sigma or TCI) were deposited by thermal evaporation, followed by 130 nm of silver (Kurt J. Lesker) also by thermal evaporation. During the C_{60} and BCP evaporations, the substrates were cooled to 0 C.

Wide Gap Single Junction Solar Cell Fabrication

Following similar cleaning as described above, ITO substrates (similar to those used above) are coated with polytriarylamine by spin coating in a dry air glovebox at 4000 RPM for 40 s (2000 RPM/s acceleration) followed by a drying step at 60 C for 5 minutes. After this, a 1.5 M solution of CsI, PbI_2, and $PbBr_2$ in 90% DMF, 10% DMSO was spread across the substrate and spun at 4000 RPM for 23 s. With 8 s remaining in the spin, 100 uL of a 0.4 M solution of FAI in 2-propanol is dripped onto the spinning substrate. After the spin, the film was annealed at 100 C for 30 minutes. Deposition of C_{60}, BCP, and a silver top electrode was as described above.

Tandem Solar Cell Fabrication

The device architecture used to fabricate monolithic tandem solar cells is similar to that described in our previous work (Eperon, Leijtens et al, Science 2016). The patterning of substrate ITO, recombination layer sputtered ITO, and top electrodes described therein allows electrical contact to be made independently to the bottom electrode (hole contact), top electrode (electron contact), or to the recombination layer.

We use thin ITO (50 nm, 40 ohm/sq) for the substrate in order to avoid parasitic absorption of near infrared light in the front ITO contact. After cleaning, a strip of 100 nm thick MgF_2 is deposited across the substrate ITO in order to avoid shunting between the edge of the sputtered ITO layer and the substrate ITO. Following this, the wide gap subcell is deposited as above. Instead of BCP and silver as the top contact, a bilayer of tin oxide and zinc-doped tin oxide is deposited by pulsed Chemical Vapor Deposition (p-CVD) as in our previous work. We then sputter a 120 nm thick layer of Indium Tin Oxide (ITO) by DC magnetron sputtering at a deposition rate of 12 nm/minute.

After the sputter, the low gap subcell stack is deposited in a similar procedure to that used for single junction solar cells.

Solar Cell Measurement

Solar cells were tested in ambient conditions without encapsulation, using an Oriel solar simulator calibrated by an NREL-certified calibrated KG-5 filtered silicon photodiode. JV curves were recorded by a Keithley 2400 source measure unit. EQE spectra were measured at short circuit using a setup comprising a white light source chopped at 73 Hz illuminating the solar cell through a 50-50 beam splitter. The split beam was directed to a silicon reference photodiode to

account for any variations of power output from the lamp. Current in the solar cell and the reference photodiode at the chopping frequency was measured by two lock-in amplifiers (Stanford Research Systems SR830) in low-noise mode.

Absorption and Band Gap Measurement

Absorption spectra of perovskite films on glass substrates were measured in an integrating sphere (LabSphere). A mercury arc lamp coupled through a monochromator (Newport) was used for illumination, with light being coupled into the integrating sphere by an optical fibre. A silicon photodiode (Newport) fitted to a port on the integrating sphere was used to measure light absorbed. The light source was chopped at 136 Hz and the photodiode current was measured by a lock-in amplifier (Stanford Research Systems SR830). A beamsplitter in the path of light before entry into the sphere was used to couple part of the light into a reference photodiode, to account for any variations in power output of the lamp.

Absorption spectra measured in the integrating sphere were used to make Tauc plots of $(\alpha h\nu)^2$ vs $h\nu$, where α is absorption coefficient, h is Planck's constant, and ν is frequency. Tauc plots of all perovskite compositions were found to have a clear linear onset, which was fitted and the intercept on the energy axis taken as the direct band gap of the material.

Table S1: Device performance of solar cells reported in this study.

Device	V_{oc} (V)	J_{sc} (mA cm^{-2})	Fill Factor	Stabilized PCE
Low gap single junction $FA_{0.75}Cs_{0.25}Sn_{0.5}Pb_{0.5}I_3$ (Untreated)	0.72	27.6	0.66	13.1
Low gap single junction $FA_{0.75}Cs_{0.25}Sn_{0.5}Pb_{0.5}I_3$ (MACl + FAH treated)	0.76	27.6	0.74	15.6
Wide gap single junction $FA_{0.6}Cs_{0.4}Pb(Br_{0.3}I_{0.7})_3$	1.14	15.8	0.78	14.5
Monolithic perovskite-perovskite tandem	1.81	14.8	0.70	19.1

Supplemental Figures

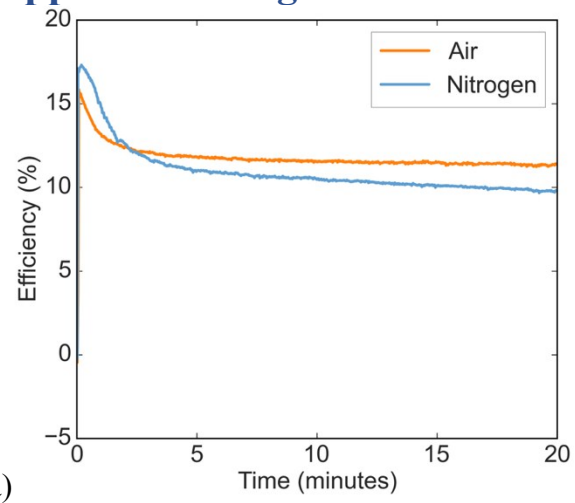

(a)

Figure S1: (a) Maximum power vs time of $FA_{0.6}MA_{0.4}Sn_{0.6}Pb_{0.4}I_3$ solar cells under continuous operation under 1-sun illumination in either nitrogen or air environments.

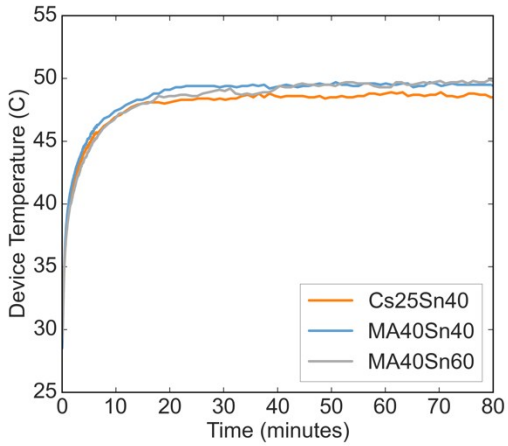

Figure S2: Temperature of devices under continuous operation at maximum power under 1-sun illumination. Cs25Sn40 refers to the composition $FA_{0.75}Cs_{0.25}Sn_{0.4}Pb_{0.6}I_3$, MA40Sn40 to $FA_{0.6}MA_{0.4}Sn_{0.4}Pb_{0.6}I_3$, and MA40Sn60 to $FA_{0.6}MA_{0.4}Sn_{0.6}Pb_{0.4}I_3$

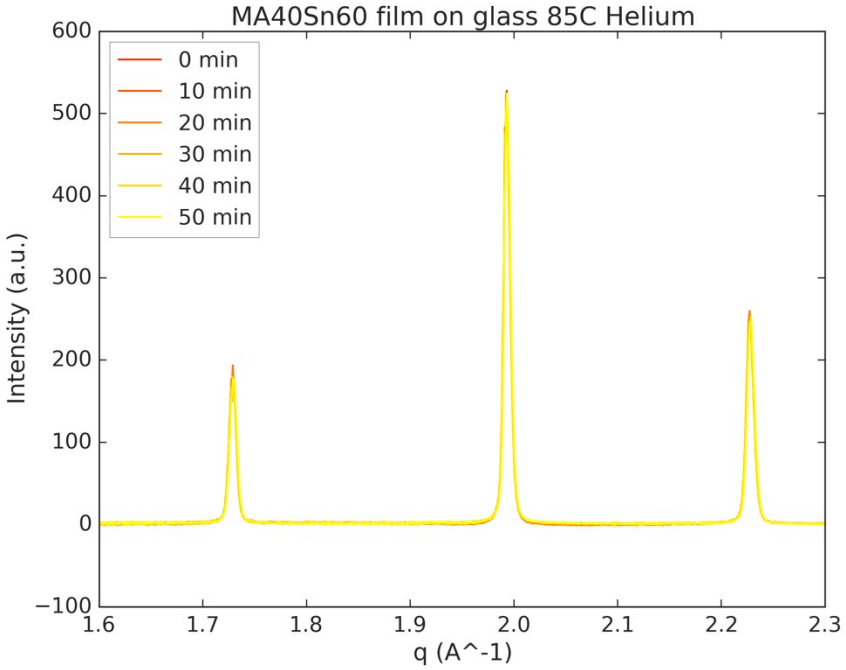

Figure S3: XRD patterns of a film of $FA_{0.6}MA_{0.4}Sn_{0.6}Pb_{0.4}I_3$ perovskite on glass held at 85 C in inert atmosphere

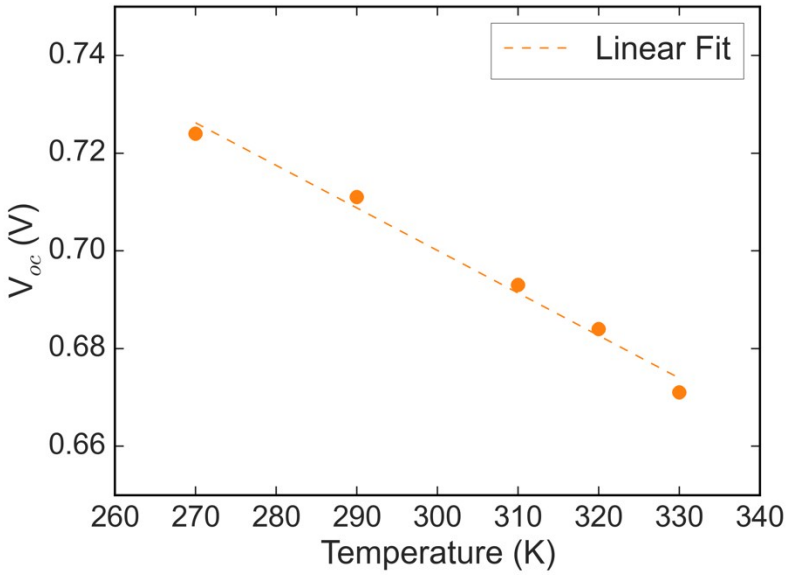

Figure S4: Temperature dependence of V_{oc} for a tin-lead perovskite solar cell with a lowered tin content (30%), $FA_{0.75}Cs_{0.25}Sn_{0.3}Pb_{0.7}I_3$. The linear fit to the data shows a temperature coefficient of V_{oc} of -0.87 mV/K.

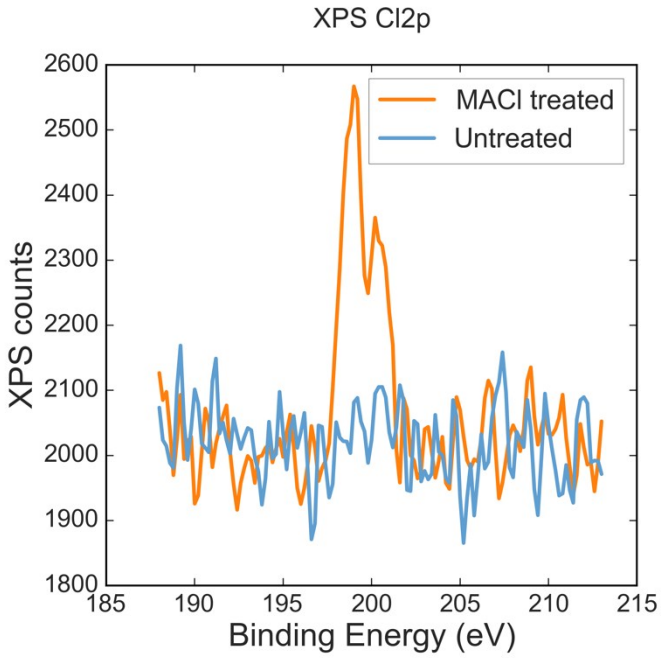

Figure S5: X-ray Photoelectron Spectra in the Cl2p region of films of $FA_{0.75}Cs_{0.25}Sn_{0.5}Pb_{0.5}I_3$ perovskite with and without post-treatment with methylammonium chloride (MACl) vapor.

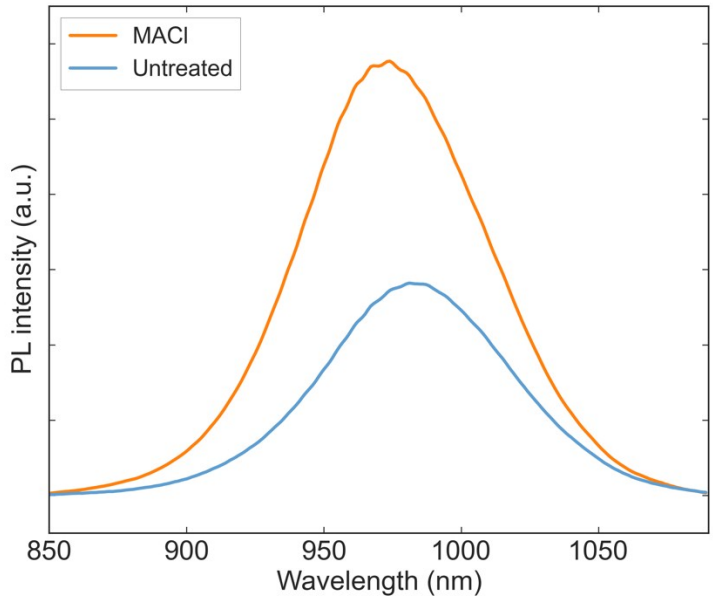

Figure S6: PL spectrum of a full $FA_{0.75}Cs_{0.25}Sn_{0.5}Pb_{0.5}I_3$ devices at open circuit with and without post-treatment with methylammonium chloride (MACl) vapor.

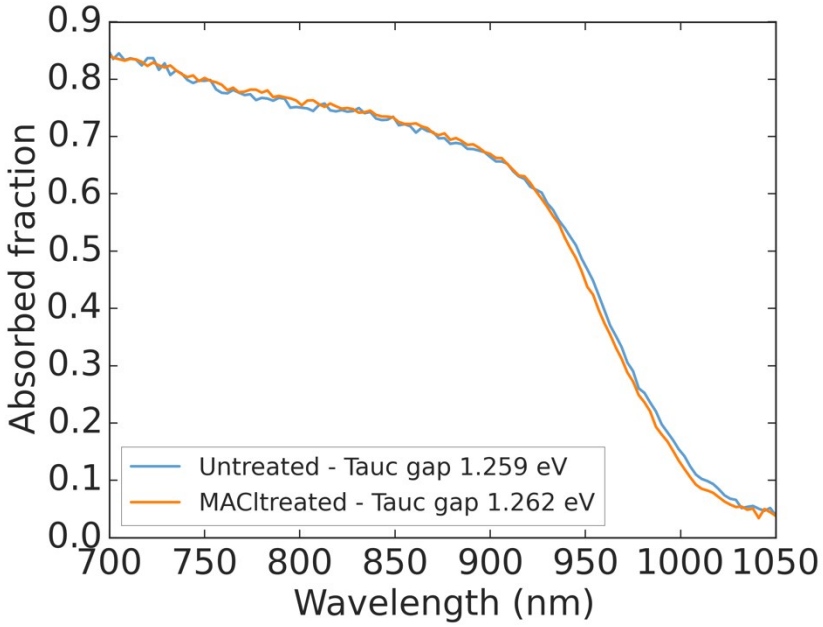

Figure S7: Absorption spectra of films of $FA_{0.75}Cs_{0.25}Sn_{0.5}Pb_{0.5}I_3$ perovskite films on glass with and without post-treatment with methylammonium chloride (MACl) vapor.

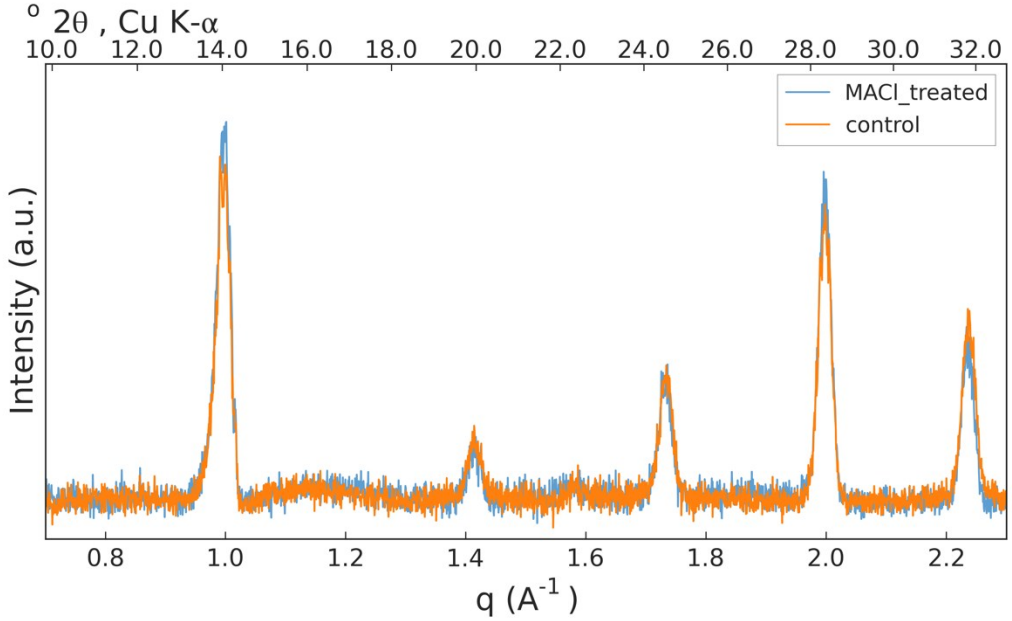

Figure S8: X-ray Diffraction patterns of films of $FA_{0.75}Cs_{0.25}Sn_{0.5}Pb_{0.5}I_3$ perovskite films on glass with and without post-treatment with methylammonium chloride (MACl) vapor.

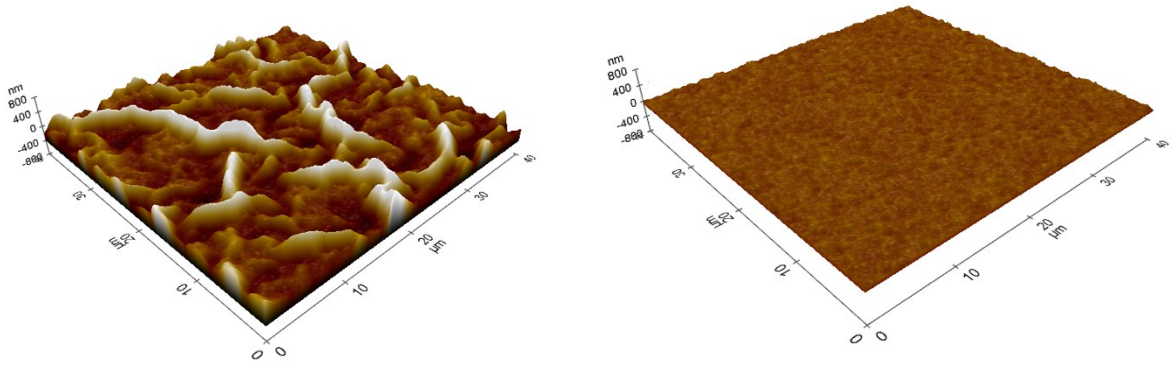

(a) (b)

Figure S9: AFM images of $FA_{0.6}Cs_{0.4}Pb(Br_{0.3}I_{0.7})_3$ wide gap perovskite. (a) wrinkled, processed by one-step spin coating, and (b) smooth, processed by the dynamic interdiffusion method developed in this work. Both images are plotted on the same scale bar for ease of comparison.

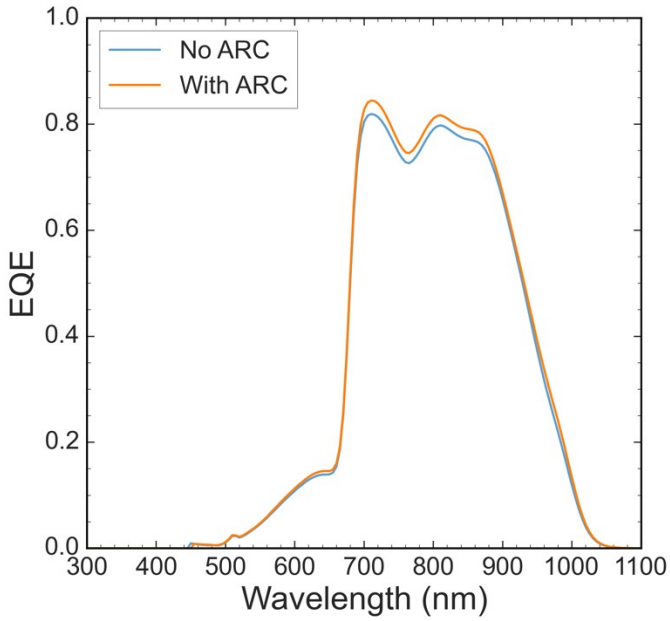

Figure S10: EQE curve of the low gap subcell in the monolithic two-junction tandem with and without an antireflective coating of magnesium fluoride (190 nm) on the glass substrate facing the light.

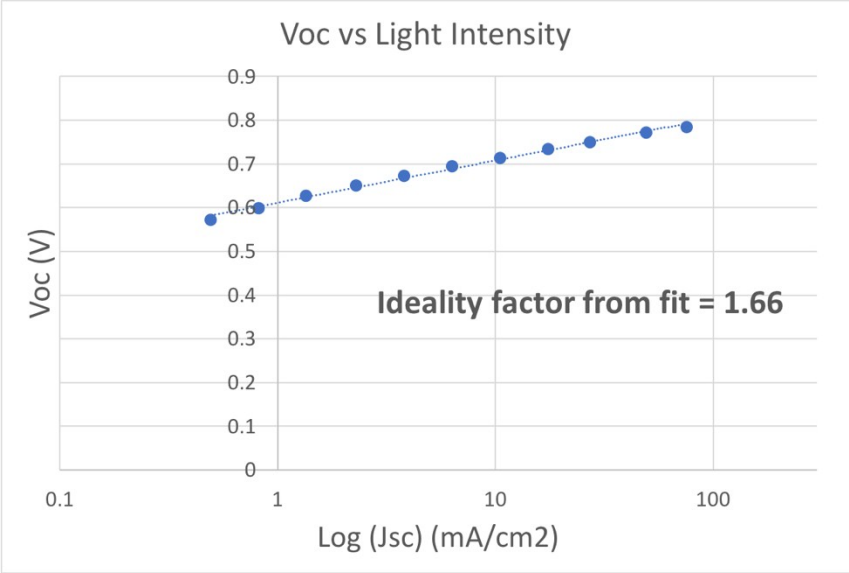

Figure S11: V_{oc} as a function of log(J_{sc}) for a $FA_{.75}Cs_{.25}Sn_{.5}Pb_{.5}I_3$ solar cell (processed identically to the low gap subcell in the tandem, with MACl vapor treatment and formic acid addition).

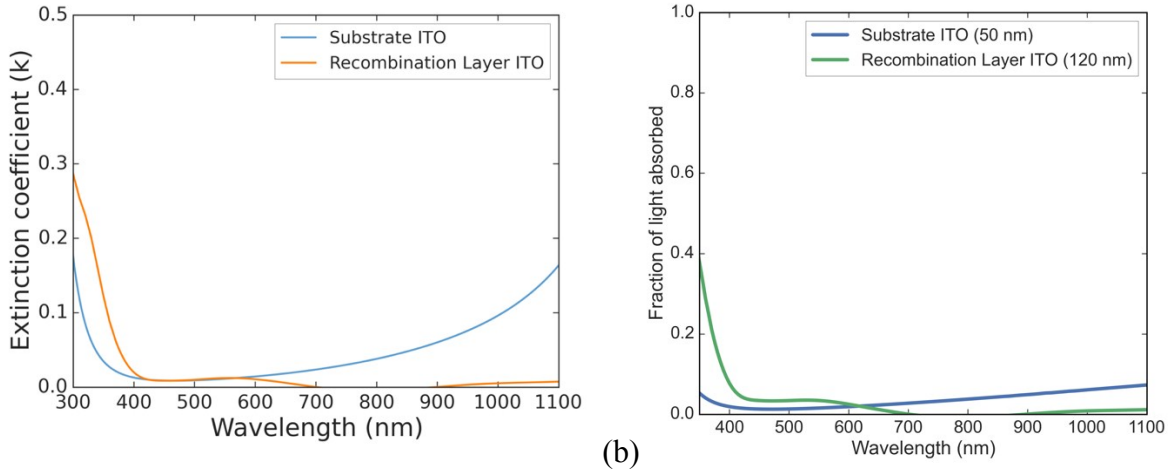

(a) (b)

Figure S12: (a) Extinction coefficient of the ITO used as the substrate vs that of the sputtered ITO used as the recombination layer. (b) Calculated fraction of light absorbed in a layer of substrate ITO or a layer of recombination layer (sputtered) ITO on glass. Calculated using transfer matrix modelling.

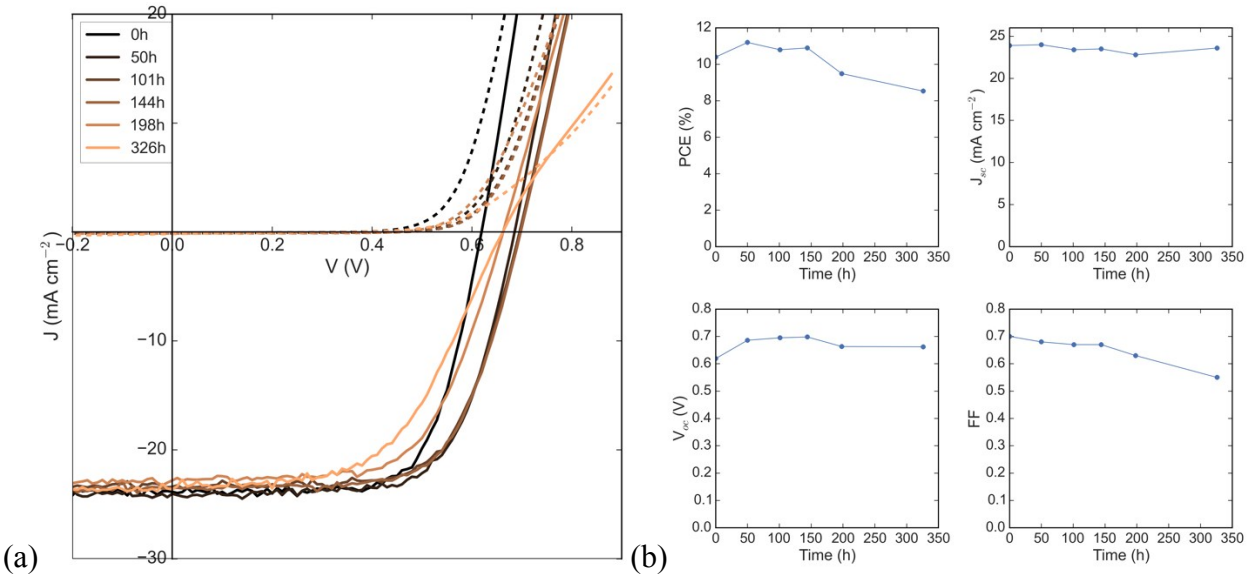

(a) (b)

Figure S13: (a) Evolution of the JV curve of a $FA_{0.75}Cs_{0.25}Sn_{0.5}Pb_{0.5}I_3$ ITO-capped device under long times of aging at 85 C in air. (b) J_{sc} vs time of this device.